Research Article

Tourmaline occurrence and gold mineralization at a granitoid-metasediment contact in the Upper Lom Basin, east Cameroon

Nicoline Kibong Fontem[1] · Cheo Emmanuel Suh[1,2] · Ralain Bryan Ngatcha[1] · Elisha Mutum Shemang[3] · Akumbom Vishiti[4,5] · Erik Melchiorre[6] · Albert Nih Fon[2]

Received: 9 September 2022 / Accepted: 30 March 2023
Published online: 18 April 2023

Abstract

Gold mineralization of the Upper Lom Basin in the eastern Cameroon goldfield is spatially associated with tourmaline. The goldfield belongs to the Adamawa-Yadé Domain of the Central African Fold Belt and is characterized by eluvial, alluvial and lode gold deposits of Pan-African age. This paper examines the chemistry and morphology of saprock gold and its link with tourmaline in the host rock. Tourmaline chemistry was obtained using the electron microprobe analysis (EMPA) technique while gold grains were examined for morphology and microchemistry using the EMPA equipped with scanning electron microscopy and energy dispersive spectrum instruments. The tourmaline compositional data plot in the dravite field, and belongs to the alkali group showing major element variations that are typical of tourmaline associated with granite-related orogenic gold deposits common along shear zones. Gold alloy composition (Ag, Cu) suggests multiple gold precipitation events due to episodic fluid influx, with a range of 572–1000 gold fineness. We infer that tourmaline development and gold deposition were coeval within the aureole around the pluton and involved reduced hydrothermal fluids with low salinity. The high $\delta^{11}B$ in the tourmaline also points to fluid derivation from the Pan African granitic basement widely recognized to be fertile in gold in eastern Cameroon. Tourmaline textural-chemical features such as low Na content and gold microchemistry point to granite-related hydrothermal style of primary gold mineralization, and has implications for exploration as tourmaline-rich rocks in the vicinity of the felsic plutons in the Lom Basin would be optimal target areas for future exploration.

Article Highlights

- Tourmaline occurs as disseminations in quartz-tourmaline veins and metasediments aureole around felsic plutons in the Upper Lom Series, eastern Cameroon.
- The textural features, dravite and alkali group compositional trend characterize hydrothermal tourmaline from granite-related and orogenic gold deposits

Supplementary Information The online version contains supplementary material available at https://doi.org/10.1007/s42452-023-05358-z.

✉ Nicoline Kibong Fontem, fontemnicolines1@gmail.com | [1]Department of Geology, Mining and Environmental Science, The University of Bamenda, P.O. Box 39, Bambili, North West Region, Cameroon. [2]Economic Geology Unit, Department of Geology, University of Buea, P.O. Box 63, Buea, Cameroon. [3]Department of Earth and Environmental Sciences, Botswana International University of Science and Technology, Private Bag 16, Palapye, Botswana. [4]Department of Civil Engineering, The University Institute of Technology (IUT), University of Douala, P.O. Box 8698, Douala, Cameroon. [5]Laboratory of Geosciences, Natural Resources and Environment, Department of Earth Sciences, Faculty of Science, University of Douala, P.O. Box 24157, Douala, Littoral Region, Cameroon. [6]Department of Geology, California State University, 5500 University Parkway, San Bernardino, CA 92407, USA.

- Gold microchemical features tie with the interpretation of hydrothermal-orogenic style of primary lode mineralization.
- Tourmaline-rich rocks in the vicinity of the felsic plutons in the Lom Basin would preferably be target areas for future exploration.

Keywords Tourmaline · Boron · Geochemistry · Gold · Sap rock · Granite-related gold mineralization · Eastern Cameroon

1 Introduction

Tourmaline is a complex borosilicate mineral and the main host of boron in crustal rocks [1, 2]. Although it is common in (meta) psammitic-pelitic rocks with B-retention minerals, it is also found in felsic plutons and their metamorphic aureoles especially in zones of continental collision where B flux is high [3]. Tourmaline is an ideal monitor of the local boron flux in metamorphic environments and can serve as a sink or source of boron [1, 4–7]. It is stable over a broad pressure and temperature range making it an important petrogenetic indicator mineral. In orogenic gold systems, tourmaline is a prominent accessory mineral that typically grows concurrently with gold mineralization. The study of tourmaline may yield useful information on the geology of a region and, by extension, on the processes that govern its growth and, ultimately, the precipitation of ore minerals like gold. Tourmaline has a wide spectrum of chemical components it can integrate because of its intricate crystal structure. This makes tourmaline a good geochemical tracer, able to show the metallogenesis of hydrothermal and metamorphism-related deposit. Consequently, it is a strong mineral indicator of orogenic gold deposits and magmatic-hydrothermal to metamorphic-metasomatic processes. Tourmaline chemical composition can provide exploitable information on the source and evolution of ore fluid [2, 7–9], including possible fingerprints on the origin of associated gold mineralization [10]. The elemental composition of tourmaline, including boron isotopic data, have been widely employed in studies aimed at unraveling: (1) The source of the boron, (2) Fluid-rock interaction processes and transport, (3) The evolution of the magmatic fluid, (4) Temperature of the fluids related to B-metasomatism, and (5) The influence of magmatic-hydrothermal process on formation of orogenic gold deposits and the timing of magmatic, metamorphic and hydrothermal processes [1, 5, 6, 11–14]. The relative abundance of $\delta^{11}B$ in nature [~ 60%; 5] makes the boron isotope system a valuable tracer of boron source in magmatic-hydrothermal and metamorphic systems [14]. There is a plexus of views on the source of fluid and metals in hydrothermal and orogenic gold deposits based on the interpretation of $\delta^{11}B$ isotopic data and the geologic setting of such gold deposits in the world [15]. A metamorphic source of fluid associated with boron metasomatism is now widely considered to be the major source of mineralizing fluids in orogenic gold deposit systems, derived from prograde to peak metamorphic devolatilization of metasedimentary basement units [16, 17]. Some authors also invoke a magmatic origin for fluids and metals related to magmatic intrusions [18], although several studies on the source of fluid and base metals in orogenic gold deposits are suggestive of a mixed magmatic, metamorphic, and meteoric source [12, 16, 18, 19]. Detailed petrographic and tourmaline composition studies are able to decipher between tourmaline that crystallized directly from felsic magmatic melt and those resulting from dehydrating fluids of the surrounding metasedimentary rocks and this has implications for metals exploration.

Cameroon is endowed with significant gold occurrences. Currently gold is mined from alluvial, eluvial and lode systems. Lode gold mineralization in the Lom Basin is largely considered to be either orogenic or granitoid-related (both with aspects of hydrothermal overprint) and occurs within quartz veins hosted by Neoproterozoic metasedimentary rocks and as veins and disseminations within the margins of hydrothermally altered granitoid intrusions, all related to the Central Cameroon Shear Zone (CCSZ; Fig. 1a) north of the Congo Craton [20–26]. Granitoid rocks accompanying gold mineralization in eastern.

Cameroon are oxidized, I-type, sub-alkaline, high-K calc-alkaline to shoshonite in composition [20, 22–25, 27]. This highlights the role the granitoids composition and redox conditions play in understanding the composition and characteristics of the exsolved ore-bearing aqueous fluids [28]. Sporadic gold deposits of low grade are also reported in quartz-tourmaline veins and quartz tourmaline microbreccia, and interpreted as the product of a boron-rich residual fluid ore concentration phase developed at the pneumatolytic stage of the evolution of the granitoids [29]. Gold exploration efforts worldwide increasingly rely on morphological studies of placer and residual gold grains, their chemical composition and mineral inclusion to fingerprint the primary source of gold and style of mineralization in most geologic settings e.g. [23, 30–34]. The core composition of gold grains and mineral inclusions entombed in them may provide vital clues on the primary lode source and its mineralogical make up [31, 35]. Employing this technique of microchemistry of residual gold grains has yielded critical findings in the

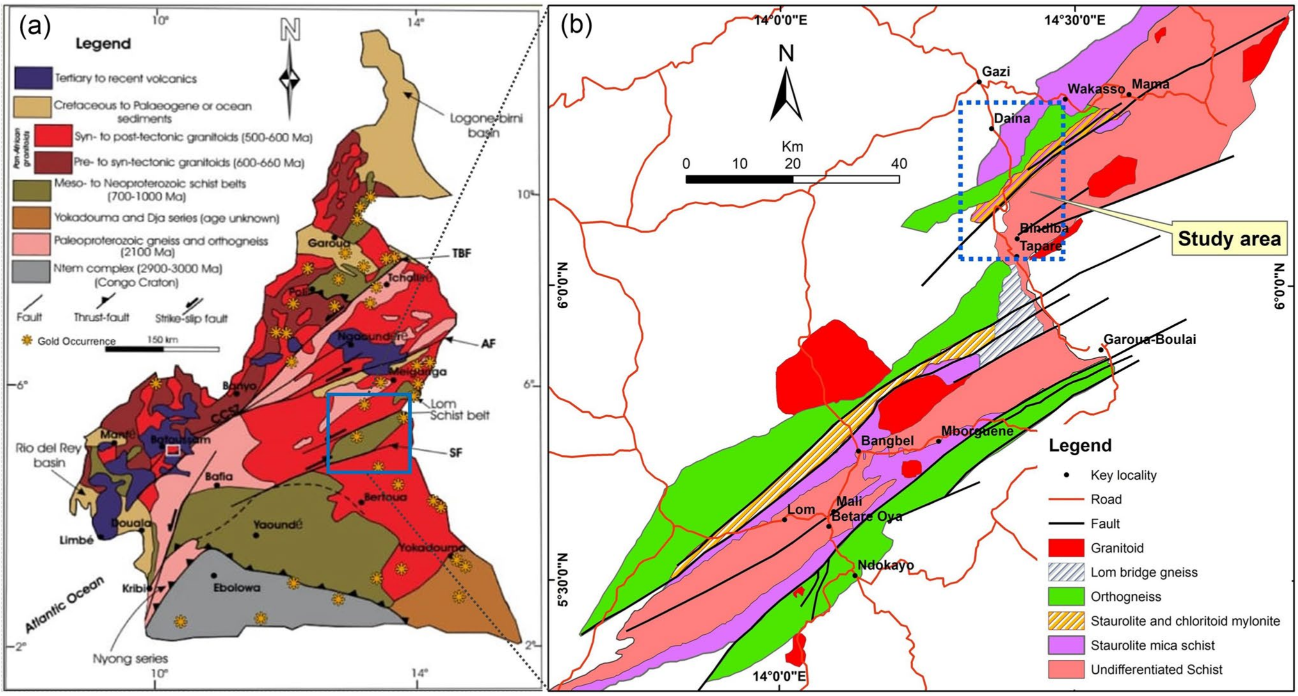

Fig. 1 **a** Geologic map of Cameroon showing the main lithostructural domains of the Neoproterozoic Pan-African orogenic belt and location of the Lom Basin, [adapted from; 59]. CCSZ, Central Cameroon shear zone; TBF, Tcholire Banyo Fault; SF, Sanaga Fault; NWC, North western Cameroon Domain (3); AYD, Adamawa-Yade Domain (2); YD, Yaoundé Domain (1). **b** Geologic map of the Lom pull-apart Basin with shear zones trending NE-SW, [adapted from 33]

identification of primary mineralization [35, 36]. The identification of primary gold deposits in the eastern, southern, and northern goldfields in Cameroon, on the basis of gold microchemistry, has yielded pertinent information concerning primary gold mineralization. Orogenic primary gold mineralization is suggested in the southern goldfield of Cameroon [21, 37–39], based on placer gold studies. Hydrothermal quartz vein style of mineralization is common in the eastern and northern gold terrane as the possible primary source of gold [21, 22, 34, 40]. In order to enhance the understanding of the style of primary gold mineralization in eastern Cameroon inferred from residual gold microchemistry, there is need to also evaluate wall-rock mineralogy such as tourmaline in combination with associated gold composition. This is the focus of this study.

Establishing a link between tourmalinization and gold mineralization in the Lom Basin of eastern Cameroon (Fig. 1b) has remained challenging due to the absence of a direct petrographic link of tourmaline co-existing with gold. However, in situ weathered material derived from tourmaline-bearing rocks is widely mined for gold in the area. Recent mining activities in the Gankoumbol-Djouzami-Beka area (Fig. 2) which is the focus of this study and lies in the upper segment of the Lom Basin has exposed underlying rocks and a thick weathered saprock-saprolite blanket (Fig. 3a and b). The saprock-saprolite material is currently being worked for eluvial gold by artisanal miners and semi-mechanized gold mining companies (e.g., Andy Saal Mining Company) and this provides the best proxy for investigating more closely the nature of gold from the underlying rocks trapped in the saprock-saprolite and the composition of the tourmaline identified therein. Weathering introduces gold and associated heavy minerals into the weathering cycle in tropical settings as in east Cameroon resulting in gold enriched haloes in the saprock and saprolite horizons. Because the texture of the primary rock is often well preserved in the saprock, minerals derived from these soil layers indicate that they co-existed within the underlying rock as the weathering cover is developed in-situ.

In this paper we use combined tourmaline composition and gold microchemistry to decipher gold metallogeny in the saprock at the contact zone of the metagranitoid and the metasediments (schist) of part of the Upper Lom Basin (the Gankoumbol-Djouzami-Beka area, Figs. 2 and 3). This undisturbed weathered material is currently accessible as it is actively exploited by semi-mechanized mining. Here we present the textural and compositional characteristics of tourmaline crystals derived from this contact zone saprock as well as the gold grain microchemistry to allow for the use of tourmaline chemistry

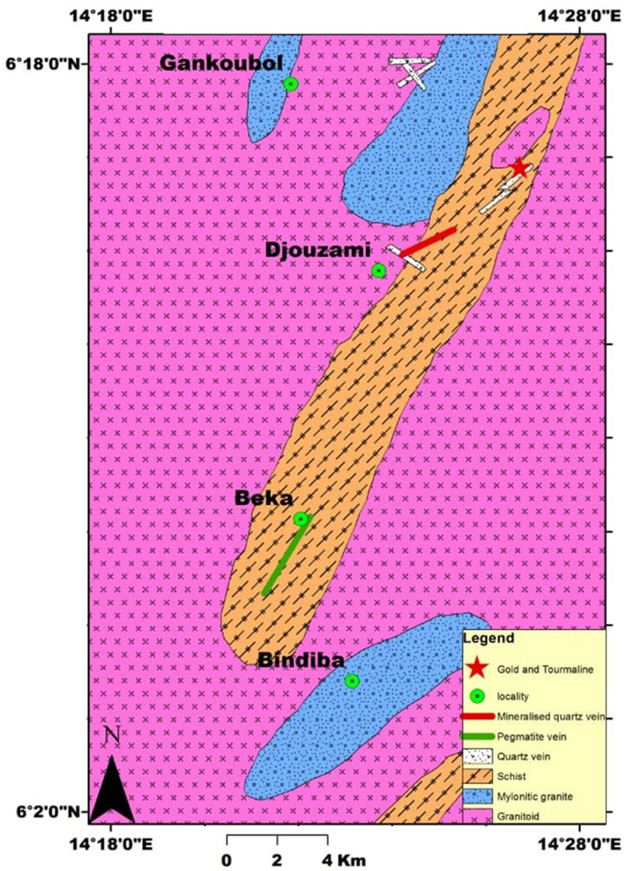

Fig. 2 Geologic map of the Gankoumbol-Djouzmi-Beka area (this study) with adaptations for the NE sector [after 60]

in lithogeochemical exploration in order to fingerprint potential primary gold host rocks in the area.

1.1 Tectonic setting and regional geology

The Pan African Fold Belt (PAFB) constitutes the southernmost branch of the Pan-African-Braziliano domain [41, 42], formed from the amalgamation of the Congo-São Francisco Craton, the West African Craton and the Sahara metacraton [41, 43], during the Gondwana assembly. This PAFB is a mobile belt known for gold and associated base metal and Ni-Co mineralization in Cameroon and neighboring countries [44]. Petrologic and isotopic data along the major shear zones in Cameroon have divided the Central African Fold Belt of Cameroon into the following lithotectonic units: (1) the North Western Cameroon Domain (NWCD), (2) the Adamawa-Yadé Domain (AYD) or Central Domain to which the study area belongs, and (3) the Yaoundé Domain, separated by major faults [Fig. 1a; 41–43, 45]. The Pan African Orogeny was accompanied by trusting to the southern edge of Cameroon and strike-slip tectonics within the PAFB that led to the development of moderate to steeply dipping strike-slip shear zones trending mostly NNE-SSW, NE-SW to ENE-WSW along the Central Cameroon Shear Zone (CCSZ) corridor (a NE extension of the Central African Shear Zone, CASZ). Several subsidiary NE-trending shear zones splay off the main shear zone (CASZ) such as: 1) the Tchollire Banyo shear zone (TBSZ) to the north, and an E-W Sanaga Shear Zone (SSZ) to the south with a N30^{o}E to N70^{o}E orientation [Fig. 1a; 43, 45–47]. The AYD is sandwiched between the SSZ to the south and the TBSZ to the north. The tectonic evolution of the PAFB involved polyphase deformation (D1-D4 phases), various degrees of metamorphism up to the granulite facies, and widespread crustal anatexis and magmatism [41]. This fold belt is associated with multiple faults and shear zones with a general NE-SW trend, with variable kinematics and representing a major lineament [43, 46, 48]. Sinistral and dextral sense of shearing characterizes the CCSZ, and granitic plutons aligned parallel to the orientation of the shear zones [46]. Gold occurrences in the eastern part of Cameroon are structurally-controlled by CCSZ and its relay faults, and associated to pluton margins [25, 26, 47]. Three deformation phases (D1-D3) are recorded in the Bétaré Oya Gold District [49] commencing with an extensional phase, followed by a collisional compressional deformation phase and terminating in a stress relaxation phase and the collapse of the orogen. These

Fig. 3 Artisanal and semi-mechanized mining in the Upper Lom Series **a** Indigenes panning and recovering gold from the exposed saprolite down to the saprock horizon. **b** Excavator exposing the saprock layer containing gold for panning

deformation events are recorded across the three litho-structural domains of the CAFB transected by the CCSZ.

The AYD is characterized by strike-slip shear zones trending generally NE-SW to ENE-WSW, with Neoproterozoic metasedimentary rocks intruded by syn- to post-tectonic granitic batholiths [20, 45, 50; Fig. 1a]. The Paleoproterozoic basement units were reworked during the Pan African Orogeny [45, 51] at varying degrees of metamorphism from greenschist through amphibolite to granulite facies [41]. The rocks of the AYD have been characterized as biotite granite, k-feldspar granite, biotite metagranite, syeno-monzogranite, granodiorite, diorite and tonalite granites of high-K calc-alkaline to shoshonitic affinities [20, 25, 47]. A number of shear zone-related lode gold mining sites in the vicinity of Pan-African granitoid intrusions have been described in the eastern part of the AYD [20, 22, 24–27, 47, 52, 53]. The ore-forming fluids are believed to have been generated during the Pan-African orogeny [41], and channeled along major lineaments into regional NE-trending shear zones and were responsible for gold and base-metal mineralization along these structures throughout the Pan-African mobile belt [54]. Previous works have attempted to constrain source of fluids and base metals in the eastern orogenic gold belt of Cameroon using stable isotopes (sulphur, oxygen, carbon, hydrogen) systematics [26, 52]. Their findings pointed to mix source (metamorphic and magmatic) of fluid [26, 52]. Tourmaline composition including boron isotopic data can provide valuable information on source and evolution of mineralizing fluids in orogenic gold systems, owing to the fact that tourmaline is a very stable mineral after crystallization, and has the ability to record and retain information of its environment of formation.

1.2 Local geology of the Lom basin

The Lom Series (Fig. 1b) is a major pull-apart basin characterized by transtensional movement [46, 48], oblique to the main shear zones (CCSZ, SFZ) and normal faults defining its eastern and western limits. It represents a sequence of metasedimentary and metavolcanic rocks of Pan-African age, including units of metatuff, volcanoclastic and sedimentary-derived schist, actinolite-chlorite schist, staurolite-garnet-mica schist and quartzite with sporadic conglomerate horizons [41, 46, 48, 55]. Metamorphic zircons from the actinolite-chlorite schist of the Lom Belt gave ages between ca. 655 and 585 Ma, implying that the metavolcanic-metasedimentary rocks of the belt were deposited prior to 655 Ma, then metamorphosed and deformed between ca. 655 and 585 Ma [56]. This event equally resulted in the development of a low-pressure garnet-andalusite-staurolite regional metamorphic mineral assemblage (greenschist-facies) [46]. Zircon U–Pb age data revealed that granitoid intrusions were emplaced within an age bracket of ca. 670–620 Ma [20, 27, 57, 58], with an average mean age of ca. 635 Ma obtained on syn-tectonic granitoid in the Bétaré Oya gold district [27], south of the present study. The granitoids recorded a metamorphic-hydrothermal overprint event between 600 and 550 Ma which could be related to the ore mineralizing fluids [58]. Geochemical and geochronological studies carried out on the granitoids in the Lom Series reveal a crustal origin with S-type [55] and I-type geochemical signatures [27, 48]. The orientation of structures and rocks in this area follow the general N50–N70 steeply dipping regional foliation (NE-SW trend of the CCSZ) related to D1 and D2 deformation phases during the Pan-African orogeny [46, 48]. The schist units (metasedimentary units) hosting some of the gold-bearing quartz veins [52] forms a NE-trending corridor, dipping steeply towards the NW and subparallel to the regional foliation. Structures within the metavolcanics and Pan-African granitoids trending NE-SW are prospective zones of economic mineralization in eastern Cameroon especially their contact zones with the metasediments [25, 44, 47].

Quartz-tourmaline veins and quartz-tourmaline micro-breccia bearing erratic gold concentrations have been reported in the Ngoura-Colomine Gold District [29]. Petrogenetic modeling from granitoids in the district suggests a preferential partitioning of incompatible elements including gold and sulphur into a residual fluid during the late stage evolution of granitoids. It is from this fluid that aplites and the gold-tourmaline-bearing structures are believed to have formed. However, detailed studies on tourmaline linked to gold mineralization in the eastern Cameroon gold are heretofore non-existent.

The Gankoumbol-Djouzemi-Beka area (latitudes 663274-700078N and longitudes 407772-444699E) investigated in this study is part of the Lom Basin (Fig. 2), with rock types including orthogneiss, metasediments (schist) mylonites intruded by variably deformed granitic plutons. Second order shear zones are common in the area and filled by quartz and pegmatitic veins (Figs. 2 and 4a). Tourmaline is associated with these veins and occurs as large subhedral crystals (Fig. 4b). The mineral also occurs as anhedral-subhedral crystals with quartz inclusions, and as disseminations within the groundmass of the meta-granitoids (Fig. 4c and d) especially around the contact with the metasediments extending into the latter. Where the deformation is strong the hinges of the microfolds in the metasediments are adorned with tourmaline crystals (Fig. 4e) and within the shear affected parts of the meta-granitoids and metasediments, tourmaline crystals are zoned, and clusters define porphyroclasts (Fig. 4f and g). Tourmaline porphyroclasts in the metasediments showing textural relationships similar to feldspar porphyroclasts

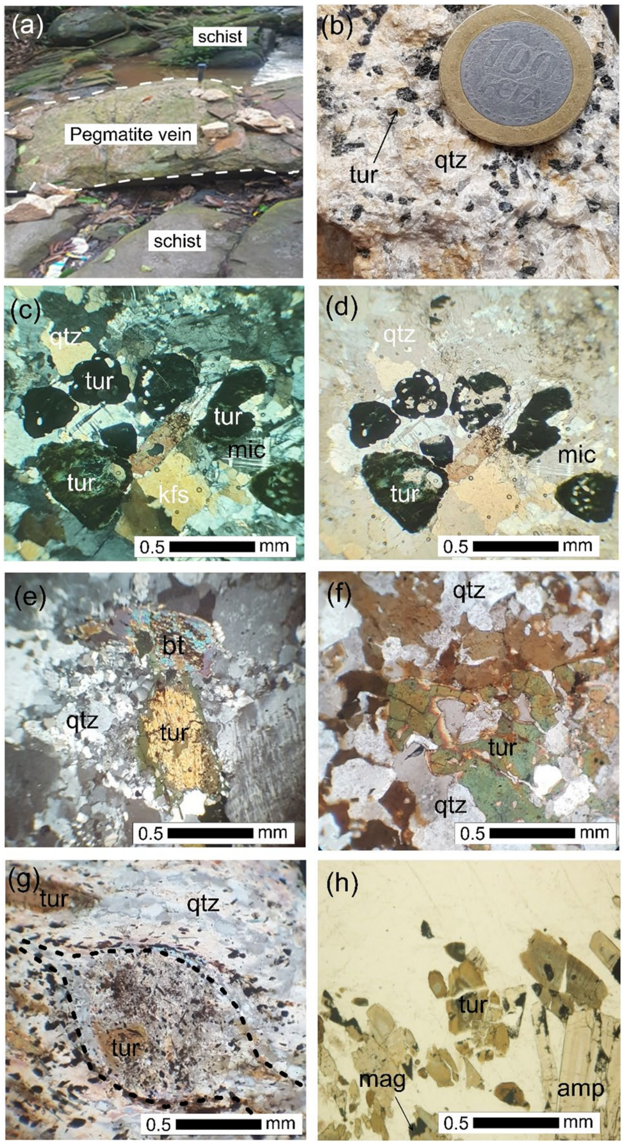

Fig. 4 Field photo and photomicrographs of tourmaline occurrences in the study area. **a** Tourmaline-bearing pegmatitic vein, field photo **b** Hand specimen sample of tourmaline needles in quartz-tourmlaine vein, **c** Tourmaline in cross polarized light, pleochroic with colour range from green–brown-yellowish, associated with recrystallized quartz subgrains in the metagranitoid. **d** Tourmaline associated with sericite in the metasediment. **e** Tourmaline crystals occupying the hinge region of the folded ultramylonite. Evidence that tourmalinzation was synchronous with ductile formation along the CCSZ (D2-D3). **f** Tourmaline showing patch zonation. **g** Tourmaline porphyroclast (augen structure) defining sinistral sense of shear with rims enveloped by opaque minerals. **h** Tourmaline on PPL associated with oxides or opaque minerals. Note that zoned tourmaline display colour variation from core to rim. Tur = Tourmaline, Qt = Quartz Kfs = K-feldspars, Amp = Amphiboles, Bt = Biotite, Opq = Opaque minerals, Ser = Sericite

(Fig. 4g) suggest that tourmaline development began prior to regional metamorphism. However, the presence of micas, epidote and quartz embayed by tourmaline is indicative of syn- to post-metamorphic recrystallization processes of preexisting tourmaline in the schist during regional metamorphism. The tourmaline crystals in the schist, metagranitoids and veins are commonly zoned (Fig. 4f and h).

2 Sampling and analytical methods

2.1 Sampling and sample preparation

Petrographic attempts to find co-existing tourmaline and gold in the bedrock within the Lom Basin have thus far been unsuccessful. In this study we examine undisturbed saprock developed in situ and overlying the metagranitoid-metasediment contact. This material contains recoverable gold grains and also tourmaline crystals, thereby serving as the most suitable proxy for studying gold-tourmaline association in the area. This saprock has been exposed by the current mining operation that targets eluvial gold in the weathering cover (Fig. 3a and b). This contact zone was also selected because the tourmaline-bearing underlying rock yielded 1.8 g/t Au and the mining operation thus far is focused on this contact and aureole around the granitoid. The saprock material was washed and panned to recover a heavy mineral concentrate from which gold grains were handpicked, packaged and shipped for analyses at University of California San Bernardino. Undisturbed saprock material (to be examined for tourmaline) was impregnated with Canada balsam, cut and 10 polished thin sections prepared therefrom. These were studied under a petrographic microscope and their composition subsequently determined by electron microprobe analyses (EMPA).

2.2 Analytical methods

2.2.1 Tourmaline Electron microprobe analysis (EMPA) and data reduction

The composition of the tourmaline crystals was determined using a CAMECA SX100 electron microprobe at the Technical University of Clausthal with analytical parameters of 25 kV accelerating voltage, 10 nA beam current, at 10 µm beam diameter size and 20 ms dwell time per pixel. The following standards were used for calibration: hematite for Fe, diopside for Ca, albite for Na, forsterite for Mg, quartz for Si, cordierite for Al, rhodochrosite for Mn, rutile for Ti, orthoclase for K, and fluorite for F. The tourmaline structural formulae were calculated from the EPMA data using an Excel spreadsheet based on the data reduction scheme in Henry et al. [61]. The tourmaline structural formulae was normalized to 15 cations in T-, Z- and Y-sites, and assuming stoichiometric composition of three atoms for B and four atoms for OH + F, based on the general formula $XY_3Z_6(T_6O_{18})(BO_3)_3V_3W$, [61], where X = Na^+, Ca^{2+}, K^+, or vacancy site; Y = Fe^{2+}, Mg^{2+}, Mn^{2+}, Al^{3+}, Li^+, Fe3 +, or Cr^{3+}; Z = Al^{3+}, Fe^{3+}, Ti^{4+}, Mg^{2+}, or Cr^{3+}; T = Si^{4+}, Al^{3+}, or B^{3+}; V = OH^-, O2$^-$ and W = OH^-, F^- or O^{2-}. The tourmaline nomenclature follows the classification proposed by [61] according to the different solid solution series, with the tourmaline chemical composition reported in weight per cent (wt%) and structural formulae are expressed in atoms per formula unit (apfu).

2.2.2 Gold grain morphology and microchemistry analyses

The gold grains recovered in the heavy mineral fraction were handpicked under a binocular microscope, embedded in epoxy resin and polished down to a 0.3 µm using diamond abrasive sequential grits to expose grain interiors following the methods described in Melchiorre et al. [62]. The morphology of the gold concentrates was obtained using the Fisher-Phenom XL Scanning Electron Microscope (SEM) to generate Secondary Electron (SE) and Backscatter Electron (BSE) images with an acceleration voltage of 15 kV. A qualitative chemical analysis of the gold concentrates was performed using an additional electron microprobe analyzer equipped with a Wavelength Dispersive Spectrometry (WDS). The WDS was calibrated to a set of purchased house standards of gold-silver-copper alloy metals prior to the concentrate analysis. Great care was taken to minimize artifacts during sample preparation, with associated errors for trace element analyses of less than ± 0.2 wt%. Au fineness was calculated using the formula [(Au*1000)/ (Ag + Au); 63].

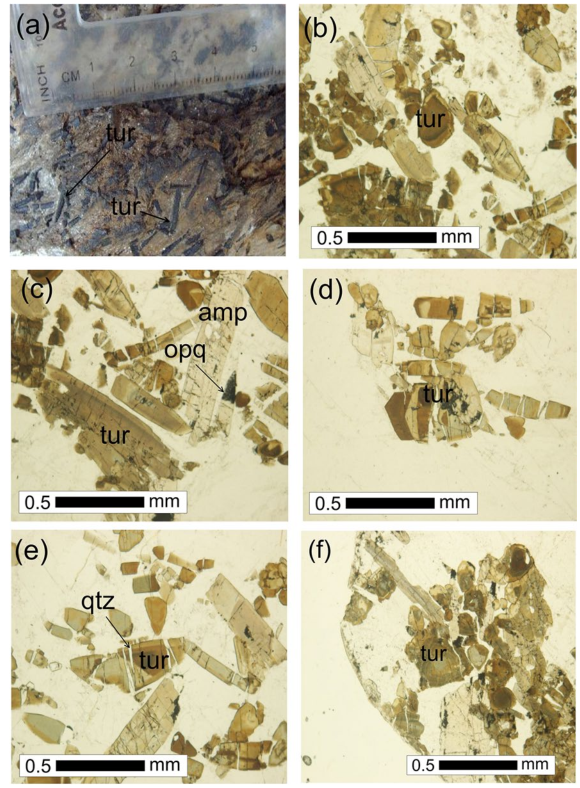

Fig. 5 Hand specimen and photomicrographs of tourmaline from the Gankounbol-Djouzami-Beka area with an emphasis on the sample material studied. (**a**) Representative hand specimen of the tourmaline enriched sample from the metasediment-granitoid contact zone (aureole) with 1.8g/t Au and slender or acicular texture, associated with K-feldspar. (**b**–**f**) are from the impregnated saprock studied: (**b**) Tourmaline in plane-polarized light (PPL) typically brown, showing patchy to oscillatory zoning, with quartz and opaque minerals inclusions. Some tourmaline aggregates are weakly zoned with cellular texture. (**c**) Tourmaline is associated with amphiboles, quartz and opaque minerals. (**d**) Tourmaline exhibiting the hexagonal crystal form zoned with opaque mineral inclusions. Note that all tourmaline crystals show evidence of brittle deformation (fractures healed with quartz and opaque minerals). (**e** & **f**) Tourmaline samples typically brown

3 Results

3.1 Tourmaline petrography and composition

The tourmaline from the material investigated in this study is described separately in the subsequent sections (Fig. 5a). Under plane polarized light, tourmaline is typically brown to orange with clear regular zoning and some crystals exhibiting a perfect hexagonal form (Fig. 5b–d). Poikilitic tourmaline porphyroclasts are equally common and contain inclusions of quartz and opaque minerals and most tourmaline grains show growth zoning with gradational colour change from core to rims (Fig. 5b and f). Some of the zoned tourmaline grains display greyish cores and thin brownish rims with few crystals having brown cores and gray to greenish rims (Fig. 5d). Cellular textures are observed in the finer tourmaline grains (Fig. 5b and f).

The chemical composition of the cores and rims of various tourmaline crystals analyzed are presented in the Table as Electronic Supplementary Material 1 alongside the substitutions in the X, Y and Z sites of the tourmaline structure. The chemical variations noted are in the range of Si 7.3–9.0 apfu, Fe 1.0–1.9 apfu, Al 5.7–8.5 apfu, Mg 1.4–2.7 apfu, and Na 0.2–0.9 apfu. Although variation in Na is relatively high, the data show low Na compared to the X-site. The Ca contents are equally low and show relatively small variations in the range of 0.1–0.5 apfu. The Ti content is low and ranges from 0.01–0.18 apfu. The contents of Mn, K and F are very low (< 0.1 wt%). The tourmaline data show high Mg/(Mg + Fe) ratios in the range of 0.4–0.7 and low Fe/(Mg + Fe) ratios of 0.34–0.52, with variable X-$_{vacancy}$/

(X-$_{vacancy}$ + Na ratios (-0.01–0.53). High Na/(Na + Ca) ratios range from 0.5 to 0.8. The values of Fe# [100* Fe/(Mg + Fe)] are not > 52.59.

Almost all the analyzed tourmaline grains plot in the field of alkali group of the schorl-dravite range (Fig. 6a) on the Ca-Xvacancy-(N + K) discrimination diagram of Henry et al. [2], showing high Al, low Fe^{3+-}, and high Mg. On the Ca-Fe–Mg discrimination diagram of Henry and Guidotti [64] the tourmaline data fall in the field of Ca-poor metapelites, metapsammites, and quartz-tourmaline rocks (Fig. 6b). These tourmalines have high Mg/Fe + Mg ratios (0.47–0.7), high Na/Na + Ca ratios (0.5–0.78) and plot in the dravite field (Fig. 7a and b). Chemical variation of tourmaline composition in metasedimentary rocks

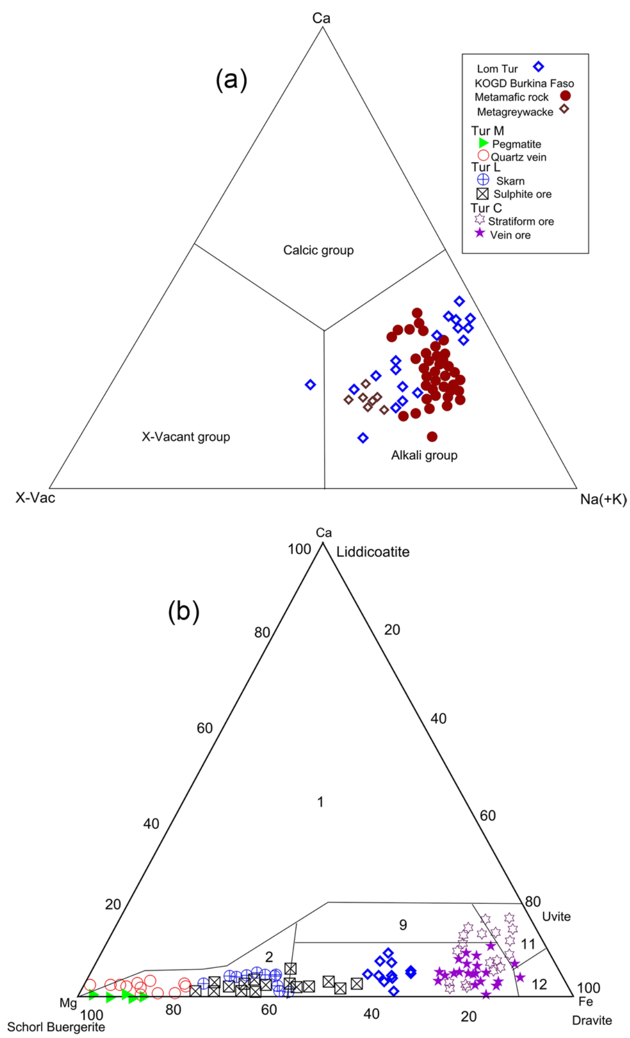

Fig. 6 Classification diagrams of the Gankoumbol-Djouzami-Beka tourmaline (Tur). (**a**) Ca-$X_{vacancy}$-(N+K) ternary discrimination plot [after 54] illustrating that the Tur belongs to the alkali group. (**b**) Ternary Ca-Fe-Mg diagraim showing the compositional variation of tourmaline [after 56]. (The studied tourmaline samples define a Ca-poor metapelites, metapsammites, and quartz-tourmaline rocks.)

and hydrothermal quartz-tourmaline veins are mostly explained by the $Mg_{+1}Fe_{-1}$ and □$Al_{+1}(NaMg)_{-1}$exchange vector joining the dravite to Mg-foitite end-members (Fig. 7c–d). All shows a positive correlation on the Al versus X-site vacancy plot (Fig. 7d) consistent with the (□Al + 1)(Na Mg2 +)-1 exchange vector. The Y site in the studied tourmaline is dominated by Mg according to structural formula calculations (Table 1). On the binary plot excess charge (Y-site) versus Fe_{tot} + Mg + X-vacancy (Fig. 7e), the tourmaline composition is above the dravite-schorl line and parallel to the (□Al + 1)(NaMg2 +)-1 exchange vector.

3.2 Gold grain morphology and microchemistry

The gold grains recovered from saprock exhibit variations in their shapes and sizes. Representative SEM/BSE images of morphology for the analyzed grains are presented in Figs. 8,9a and b. The three main grain morphologies include elongated-ellipsoidal wire-like gold, irregular, and bean shaped, with all exhibiting rough surfaces bearing cavities filled with oxides and silicates.

The representative EDS spectra of the analyzed gold grains are shown on Fig. 9a and b and the gold grain compositional data presented on Table 1. From the SEM/EDS data, the analyzed gold grains range from pure gold (100 wt%) to alloys of Au–Ag, and of Au–Ag-Cu, with Au rich rims and Ag rich cores (Fig. 9a and b). Generally, the gold grains display a wide range in Au content from 57.15 to 100 wt%, with fineness values in the range of 571–1000. The elongated-ellipsoidal gold grains have high purity gold rims (86.54-100wt% Au), lower Ag (1.43–8.48 wt%) and traces of copper compared to their lower purity cores (88.83 wt% Au, 5.72 wt% Ag, 4.82 wt% Cu). The irregular and bean-shaped gold grains show lower purity gold cores and rims (57.15–62.78 wt% Au), higher Ag (34.46–42.85 wt%) and Cu (2.76–5.45 wt%). Ag content in all the analyzed grains shows significant variation, with the highest Ag content recorded in the irregular and bean-shape gold grains (23.77–42.85wt%). The Au/Ag content varies from core to rim for the different gold grains analyzed, with copper detectable in most gold grains. This variation is observed both between different grains, and within the same grains (Table 1). The common minerals associated with the gold grains include quartz, Fe-oxide, monazite, garnet, copper oxide, ferrosilite and a niobium alloy, all of a few microns in size. On the Au–Cu–Ag discrimination diagram, the gold grain data plot in the field of hydrothermal-orogenic gold type deposit (Fig. 10). The compositional variation trend for Au, Ag and Cu for the analyzed gold grains is not systematic from core to rim (based on gold fineness and EDS spectra; Fig.9a and b).

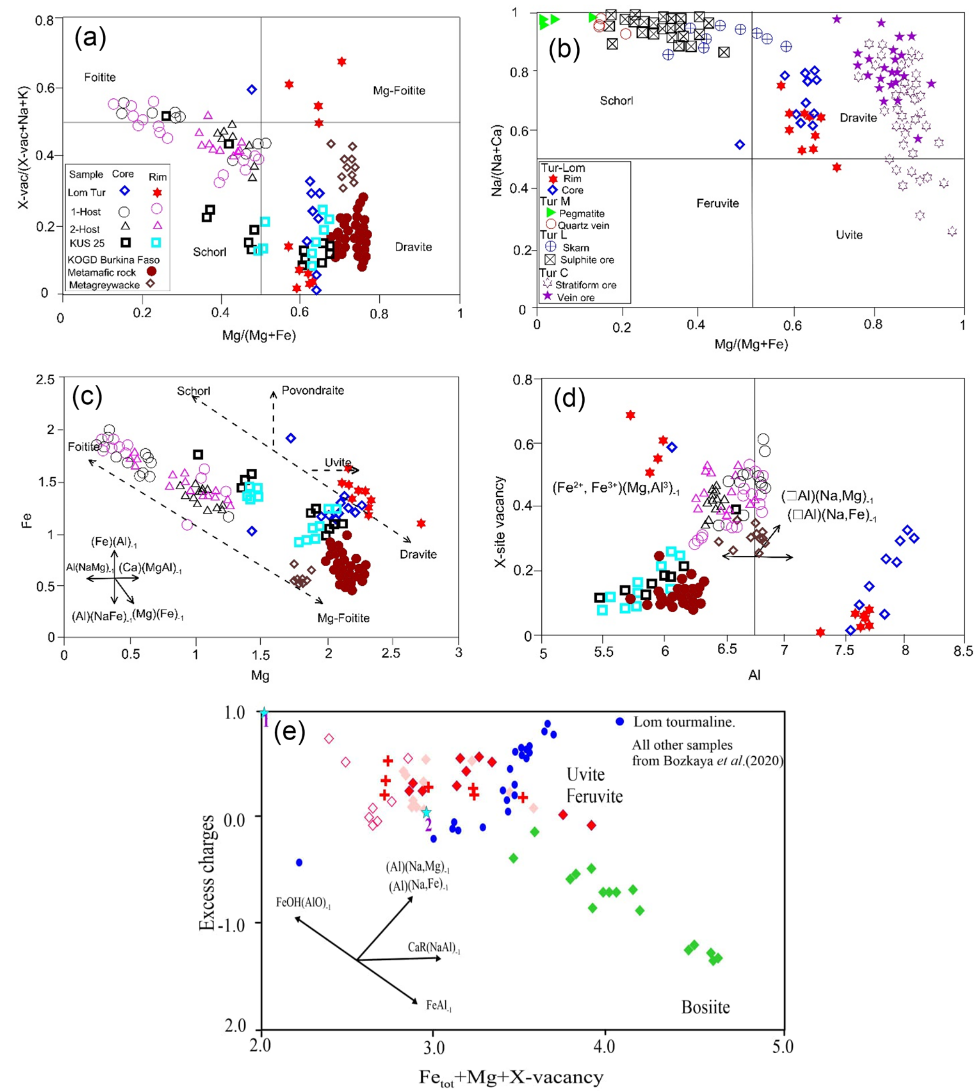

Fig. 7 **a** Classification of tourmalines from the Gankoumbol-Djouzami-Beka district based on the calculated Mg/(Mg + Fe) versus X-site Vacancy **b** Mg/(Mg + Fe) versus Na/(Na + Ca), illustrating that tourmaline belongs to the dravite field. **c** Chemical variation Binary diagram Mg versus Fe cation occupancies in tourmalines showing rich magnesium composition. **d** Binary diagram Al versus X-site vacancy of cation occupancies showing Al-rich tourmaline. The tourmaline data from this study is plotted with major element data from the Kiaka orogenic deposit, Burkina Faso and the Hattu schist belt, Finland. **e** The binary excess charge versus F_{etot} + Mg + X-vacancy diagrams illustrating tourmaline composition from the Gankoumbol-djouzami-Beka area. Upper Lom Basin. (1) X-vacancy—R2 + –O rootname (oxy-magnesio-foitite) and oxy-foitite, (2) schorl, dravite, magnesio-foitite, foitite. (The tourmaline data from this study is plotted with major element data from the Kışladağ deposit, China

4 Discussion

4.1 The tourmaline-primary gold link and ore-forming fluid

The proximity of the gold mineralization in the study area to granitic plutons and shear zones is pertinent to unraveling the origin and nature of primary gold mineralization in the area. We interpret from tourmaline abundance and similarity in textural features both in the undisturbed saprock developed in situ and overlying the metagranitoid-metasediment contact (aureole around the granitic plutons), both containing recoverable gold grains, that they were all precipitated from a similar hydrothermal fluid. From the petrographic investigations, the textural relationships are consistent with growth zoning in tourmaline [65]. Furthermore, formation of patchy zoning, pale discordant reaction rims, and multiple growth zones in tourmaline (Fig. 5b and f), are interpreted as evidence of multiple episodes of tourmaline growth [66]. Zoning irregularities and cellular textures in the fine-grained tourmaline population is possibly a product of coalescence of a number of small tourmaline crystals followed by relatively regular or discrete growth around the coalesced center. The preponderance of these cellular textures in the fine-grained tourmaline grains relative to the coarse-grained tourmaline crystals points to a greater effect of dissolution-diffusion processes on the former [3]. All of the textural features described above, resulting from post-growth dissolution-diffusion processes, formed during the hydrothermal phase. The quartz inclusions observed in tourmaline crystals and porphyritic poikiloblasts reflect a hydrothermal signature associated to its crystallization (Figs. 4c–d, 5b). The optically zoned tourmaline is typical of hydrothermal orogenic gold deposits, with

Table 1 Electron microprobe analytical data (wt%) of gold grains from the Upper Lom river channel, eastern Cameroon

Analytical points	Ag	Au	Al	Ce	Cu	Fe	Nb	Nd	O	p	Rb	Si	Zr	Total	Fineness
1							60.99		1.19	37.82		100			
2							52.04			47.06		99.1			
3	0	0		31.93	2.34	0		54.58		11.16				100.01	
4						88.3			11.7					100	
5	40.3	59.7			0									100	597
6	23.77	76.23			0									100	762.3
7							72.19			0			27.81	100	
8	7.56	89.32			3.12									100	921.96
9	14.36	80.83			4.81									100	849.14
11	13.46	86.54			0									100	865.4
12	0	100			0									100	1000
1	0	0			39.04				60.96					100	
2	5.72	88.83			5.45									100	939.50
3	0	100			0									100	1000
4			11.58			40.84			31.01			16.57		100	
5	34.46	62.78			2.76									100	572.55
6	42.85	57.15			0									100	571.5
7	39.37	60.63			0									100	606.3
8	0	100			0									100	1000
1	0	100			0									100	1000
2	4.01	92.44			3.56									100.01	958.42
3	0	100			0									100	1000
4	1.43	98.57			0									100	985.7
5	2.11	97.89			0,00									100	978.9
														0	
1	88.83	9.25			1.93									100.01	94.31
4	8.48	91.52			0									100	915.2
														0	
Map1	7.61	92.39			0									100	923.9
2	12.74	0				1.07			72.82			13.38		100.01	0

the brown zones exhibiting relatively high Fe content, while the light-gray zones show high Mg content. The major element occupancy in the crystallographic sites of tourmaline crystal with general formula $XY_3Z_6(T_6O_{18})(BO_3)_3V_3W$ [61] determines the structural formula of the tourmaline-super group minerals. These sites serve as primary parameters in the tourmaline nomenclature. Ionic variations of greatest interest occur on the X-site = Na^{1+}, Ca^{2+}, K^{1+} and □ (vacancy), the Y-site = Fe^{2+}, Mg^{2+}, Al^{3+}, Fe^{3+}, Li^{+1}, and the Z-site = Al^{3+}, Fe^{3+}, Mg^{2+} and Cr^{3+}, B = B^{3+}, T-site by Si and, V-sites by O, OH, and W-site by OH^-, O^{2-}, F^-, Cl^- [6, 7, 61]. The tourmaline data from this study (Fig. 7a and b) show affinity with Na-Mg (+ Fe) tourmalines of dravitic composition [61] common in intrusion-related gold deposits.

The major element composition of tourmaline in shear zone-related orogenic gold deposits, dominated by high fluid-rock ratio is generally buffered by the fluid phase [64]. The dominant $Mg_{+1}Fe_{-1}$ and $□Al_{+1}(Na,Mg)_{-1}$ exchange vectors (Fig. 7c and d), may be suggesting tourmaline precipitation from reduced hydrothermal fluids [15, 67]. The Mg-Fe^{2+} substitution is indicative of an insufficient proportion of Fe^{3+} in the tourmaline composition [66]. However, low Fe content in tourmaline has been demonstrated to reflect high abundance of Fe-oxides and sulfides, and indicates greater ore-forming potentials [68], or an evolution from an Fe-rich to Mg-rich variety resulting from late-stage sulphide deposition [69]. So, this maybe suggesting that lode gold mineralization in the Upper Lom Series is most likely associated with Fe-sulfides and oxides as is the case in the Lower Lom Series [26, 52]. Low Fe content can also be attributed to the precipitation of hematite [70]. The absence of Al-Fe^{3+} elemental substitution in tourmaline may suggest tourmaline crystallization from

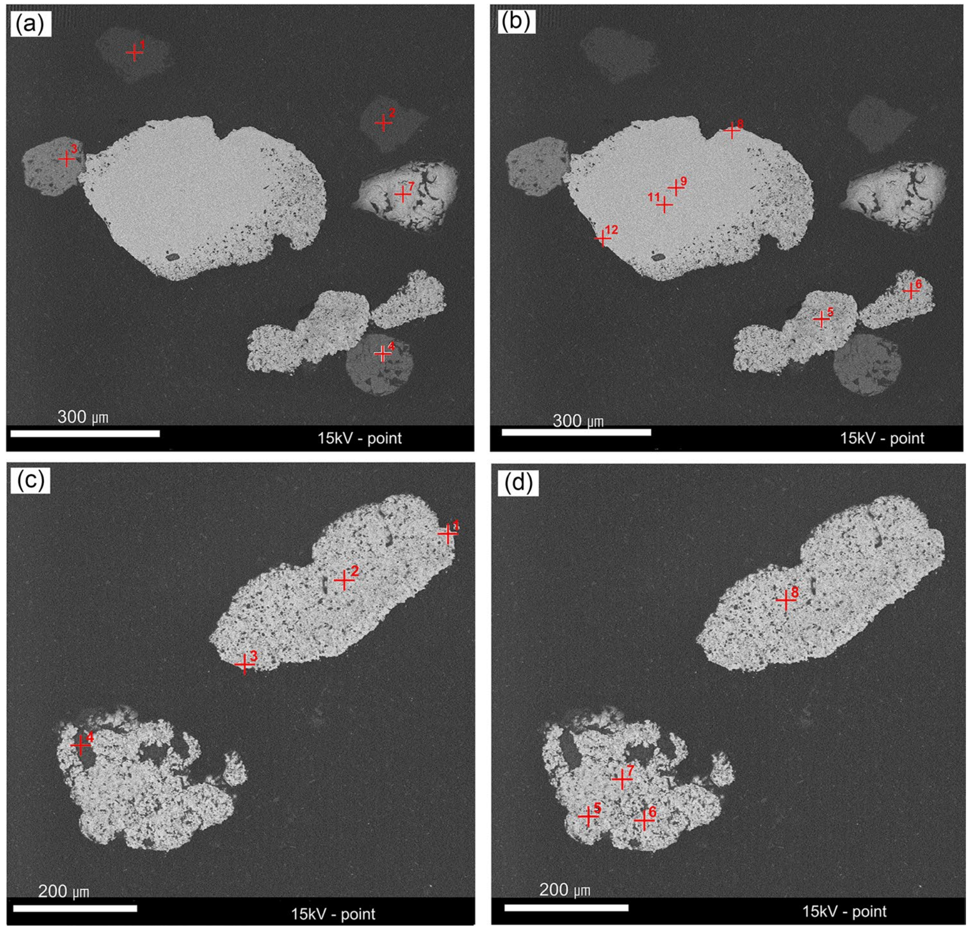

Fig. 8 BSE images of representative saprolite layer gold grains from the Gankoumbol-Djouzami-Beka area (Upper Lom Series). (**a** & **b**) Sub-rounded gold grains showing smooth surfaces pitted rims with regular outlines. The bean-shaped gold grains show pitted surfaces with regular to irregular outlines. (**c** & **d**) elongated gold grains show pitted surfaces with smooth outlines, whereas the irregular gold grains display rough surfaces with cavities filled with oxides and silicates and irregular outlines. The inserted red "X" identifies the analyzed spots

a reducing hydrothermal fluid [11]. Our data show high Mg/(Fe + Mg) ratio 0.47–0.7, low Ca content 0.18–0.47apfu, low Fe content 1.0–1.9 apfu, and low Na content 0.2–0.9 apfu, (Fig.7a–d). These results are consistent with syn-ore hydrothermal tourmaline from the orogenic gold deposit described in the Loulo Gold district in Mali [71]. Our results are also consistent with tourmaline hosted in metagreywacke in the felsic pluton linked Kaika orogenic gold deposit in Burkina Faso (West Africa) plotting in the dravite field [Fig. 7a 7 b; 15].

The occurrence of tourmaline in the saprock paragenesis at the Upper Lom Basin is an indication of the importance of boron in the original hydrothermal system responsible for the gold mineralization. Na and Ca are a function of fluid salinity as their concentrations determine the composition of the X-site in tourmaline [6]. The low Na (0.2–0.9apfu) and Ca (0.18–0.47 apfu) contents compared to the relatively high contents in X-site vacancy (0.46–1.23apfu) indicate low salinity magmatic fluid as tourmaline derived from metasediments would have higher Na content. Fluid inclusion data in the eastern Cameroon goldfields yielded similar results (~ 7.5 wt% NaCl equivalent), further supporting a granite-related source for the ore-forming fluids [26, 72]. Reported $\delta^{34}S$ (+ 6.5 to + 7.0‰) for gold-bearing pyrites from the eastern goldfield also suggests a mixed magmatic-metamorphic source for the sulfur that was involved in the precipitation of sulfide minerals. The concentrations of pyrite and tourmaline in the hydrothermal alteration zone from this study suggest a significant volatile component (H_2S, B) in the mineralizing fluid. The following conditions are proposed to control hydrothermal tourmaline precipitation and gold mineralization in the Upper Lom Series; low to moderate salinity, and reduced hydrothermal fluids.

Preliminary B isotope data (Fontem, unpublished data, n = 9) supports this granite-derived B-rich fluid as the $\delta^{11}B$ isotopic values of the tourmaline (Fig. 11) are high. Such high $\delta^{11}B$ values suggest the involvement of an I-type granitic pluton [73]. Neoproterozoic granitoids in the eastern Cameroon goldfields are also I-type metaluminous to slightly peraluminous and associated with gold mineralization [57, 58]. As an incompatible element, B is readily transported by granitic melts and hydrous fluids derived therefrom [74]. Granitic rocks emplaced along gold-bearing shear zones associated with significant hydrothermal alteration is proposed as a major source of

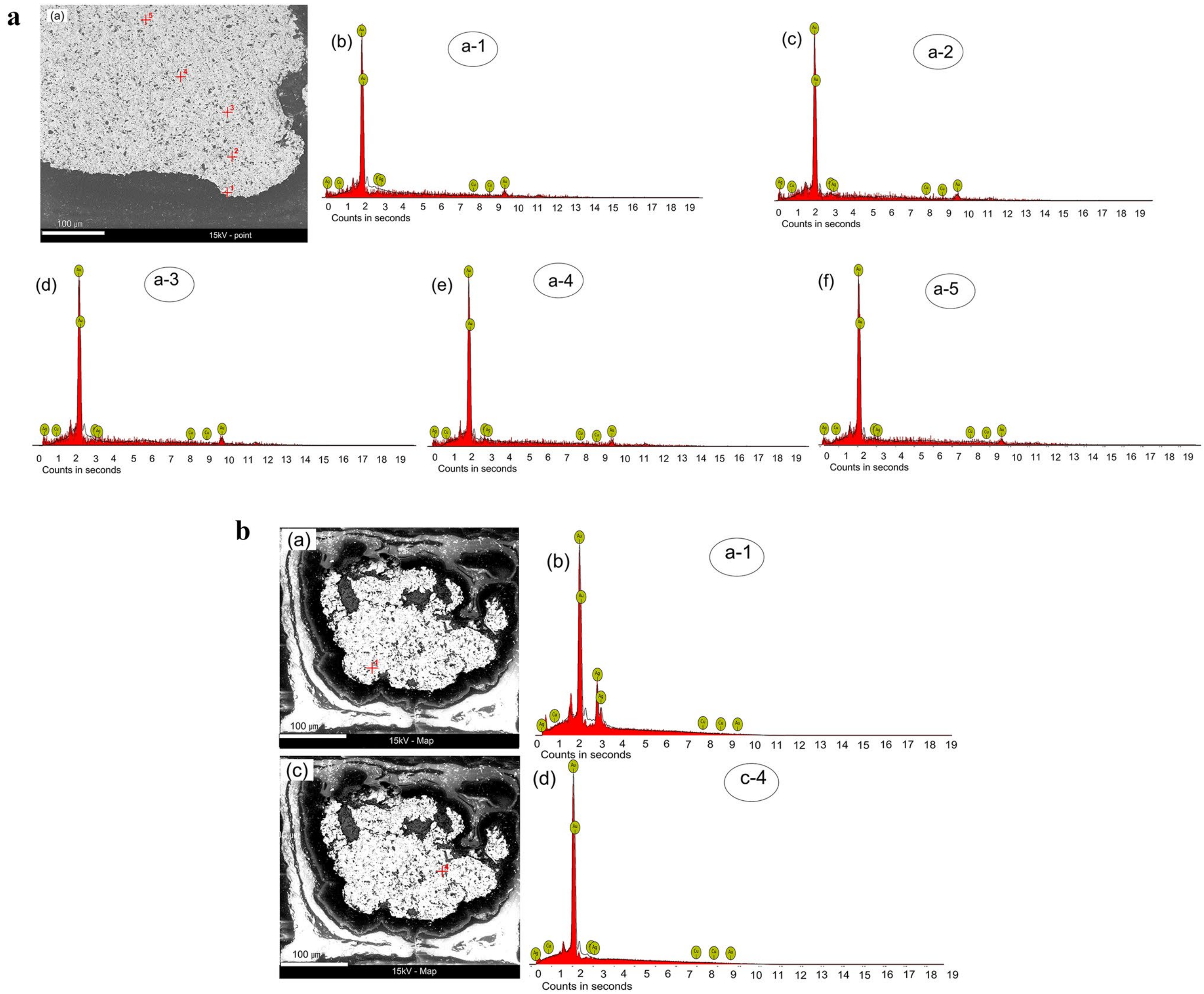

Fig. 9 SEM images (**a** & **b**) and EDS patterns of gold grains from the saprock layer

Fig. 10 Ternary diagram Au–Ag × 10 versus Cu × 100 discrimination plots of gold compositions in this study (Gankoumbol-Djouzami-Beka area, Upper Lom Basin) compared with chemical composition superficial gold deposits in eastern and northern Cameroon goldfields; Batouri eluvial gold [33], Bétaré Oya vein Au [50], Lom and Nyong alluvial gold [29], Primary gold East region, Cameroon [45], Betare Oya alluvial Au [23], Gamba district Au [26]

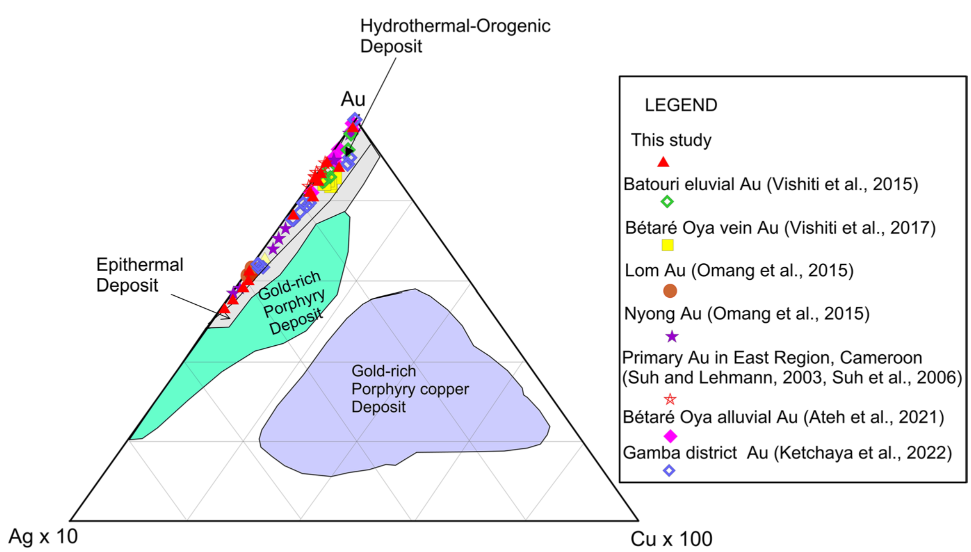

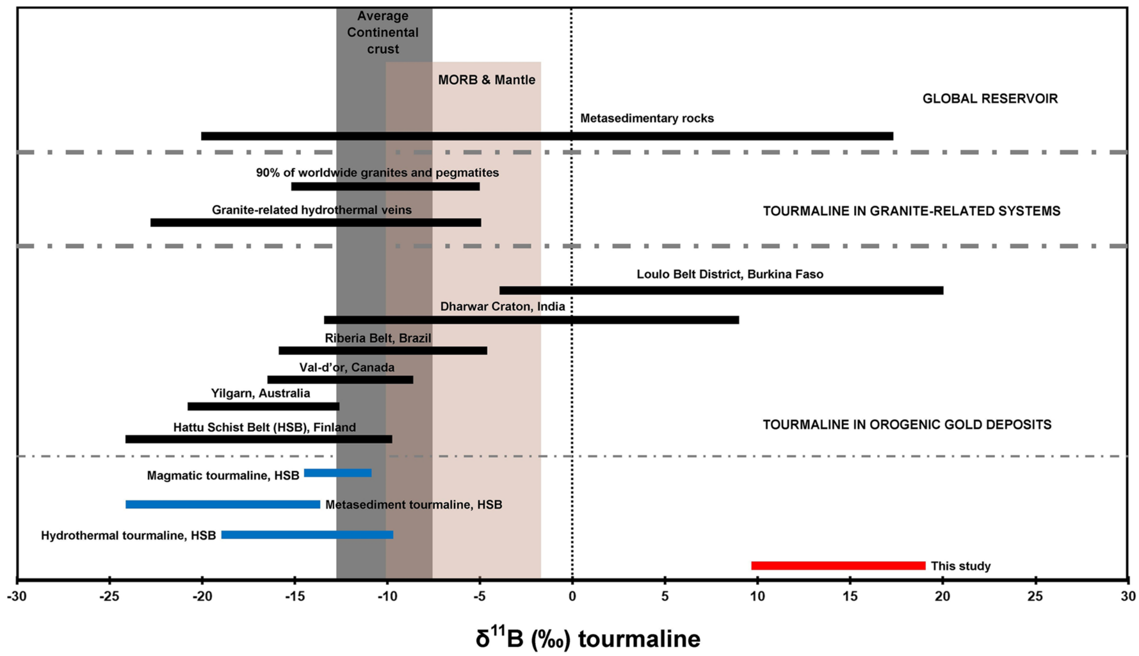

Fig. 11 Reconnaissance B isotope data (Fontem, unpublished data) for tourmaline in the studied sample compared to other deposits worldwide (Data are compiled from: [13, 19]. While more detailed isotope work is need, these data suggest granite-derived B-rich hydrothermal fluid involvement in the development of the tourmaline and possibly gold mineralization

boron-rich magmatic fluid [15]. Magmatic-hydrothermal fluids enriched in isotopically heavy boron probably dominated the formation of tourmaline [75]. Although the possibility of an external boron-enriched fluid leached from the widespread metamorphic basement rock may not be totally ruled out [52, 56] as inferred from the sulfur isotope data in the area, our B isotope data points firmly to a dominant granite derived ore-bearing fluid. Hydrothermal tourmaline can therefore be used as a suitable exploration tool for primary orogenic gold deposits.

4.2 Implications for the regional footprint of primary gold mineralization

The residual gold grains in our study show no evidence of transportation and secondary overgrowth structures. The elongated grains and pitted rims provide evidence of intense in-situ physical and chemical weathering marked by deep Ag leaching at the rims. The irregular and bean-shaped gold grains with rough outlines and cavities suggest recently dislodged grains from the bedrock into the saprock with limited weathering effect.

The microchemical classification of alluvial and eluvial gold grains is a technique that has been applied by many authors to provide information on the type, source and mode of primary gold mineralization in an area [21, 30, 34, 36, 39, 62]. Primary mineralization studies and source deposit type can be investigated using Au-alloy composition and gold grain geochemical variation [76]. The Ag content in gold grains and alloyed elements are criteria considered when interpreting gold grain microchemistry and used to determine the deposit type [76]. Core chemistry of gold grains has been interpreted to closely represent the lode gold source chemistry [62].

The chemical composition of the gold grains recovered from the saprock at Gankoumbol-Djouzami-Bekain the Upper Lom Basin shows a Au–Ag ± Cu signature. This is similar to the Au–Ag ± Cu ± Hg ± Se signature reported in the Lower Lom Basin [52]. High Ag and low Cu content is indicative of a hydrothermal-orogenic type mineralization [21, 22]. The high purity in gold content recorded in rims and cores sections of some grains (100wt. %; n = 5) is interpreted to reflect preferential Ag leaching resulting from intense in-situ chemical weathering yielding such high gold fineness (purity). The high Ag content recorded in the core and rim portions of irregular recently dislodged gold grains at the sap rock/saprolite boundary could be related to the limited physical and chemical weathering resulting to negligible Ag leaching and point to the presence of electrum, a natural alloy of gold with > 20 wt% Ag sourced from Ag-enriched primary deposit. Cu content < 1 in gold grains are usually interpreted to indicate a hydrothermal granite-related type deposit for the primary source [22]. Our data show Cu contents in the range of 1.9 to 5 wt%. These gold grains all show characteristics of hydrothermal-orogenic gold deposit type [35; Fig. 10]. Variations from pure Au, to Au–Ag alloy, and Au–Ag-Cu alloy, in the core of some gold grains equally suggests multiple episodes of gold precipitation events from a voluminous fluid system during the primary gold deposit emplacement. Thus, the primary lode is plausibly a hydrothermal gold deposit type with primary mineralizing fluids sourced from the felsic intrusions as evidenced by the B-isotope data. Previous studies in the eastern goldfields in Cameroon are suggestive of the fact that primary gold mineralization is typically of intrusion-related gold deposit setting [24, 25], with gold remobilized from early magmatic sulphides by fluids and concentrated along shear zone [25]. The Au alloy composition is both binary (Au–Ag) and ternary (Au–Au-Cu). This may attest to slight changes in hydrothermal composition (e.g., salinity, pH, Eh, temperature) during hydrothermal fluid evolution. These findings are consistent with results of previous researchers in eastern Cameroon [21–23, 37, 38, 47].

4.3 Implications to metallogenesis and gold exploration targets

Tourmaline textural and chemical features as well as gold microchemical characteristics point to an orogenic-hydrothermal style primary gold mineralization in this area. Although previous studies have suggested mixed magmatic-metamorphic hydrothermal fluids responsible for gold mineralization in this area, our B isotope data clearly points to a granitic source. This has implications for metallic resource exploration as tourmaline-rich rocks in the vicinity of the felsic plutons in the Lom Basin would preferably be target areas for future exploration.

5 Conclusion

This study was designed to investigate the link between B metasomatism expressed as tourmaline formation, and gold mineralization in the aureole of a granitic pluton. We demonstrate here that the black tourmaline in the Gankoumbol-Djouzemi-Beka area in the Upper Lom Basin occurs as disseminations in gold-bearing quartz-tourmaline veins, and as metasomatic-hydrothermal replacement tourmaline at the granitoid-metasediment contact and alteration zones hosting 0.6–1.8 g/t Au. The tourmaline-bearing veins trend NE-SW crosscutting the metasediment country rock, and straddling granite-metasediment margins. The hydrothermal tourmaline data in this study show affinity with the alkali group with a dravitic composition. $\delta^{11}B$ isotope values of the tourmaline are high suggesting the involvement of granitic plutons in the area. This is consistent with low Na content in the tourmaline. The high purity in gold content recorded in rims and cores sections of some grains (100wt. %) is interpreted to reflect preferential Ag leaching resulting from intense in-situ chemical weathering. The high Cu content in the gold grains probably points to a hydrothermal-orogenic gold deposit type with high fluid-rock interaction resulting from episodic fluid influx. This is also reflected in the Au-alloy composition (Ag, Cu), suggesting multiple episodes of gold precipitation events from an evolving fluid system. Tourmaline morpho-chemical features and gold microchemistry points to an orogenic-hydrothermal style of primary gold mineralization in this area, and has implications for gold exploration as tourmaline-rich rocks in the vicinity of the granitic plutons in the Lom Basin would preferably be target areas for future exploration. The limitation of the study lies in the relatively restricted number of tourmaline grains analyzed for B isotope. More data on the various forms of tourmaline in the metasediment and the granite away from the contact zone investigated in this study should throw more light on the diversity of tourmaline and B sources in the region.

Acknowledgements This paper is part of the PhD thesis of the first author in progress at The University of Bamenda. CES, EMS and EM acknowledge the collaboration framework through which the data reported here were acquired. CES acknowledges with thanks the analytical support of Klaus Herrman with the EMPA analyses completed through the diligent support of Prof. Bernd Lehmann of TU Clausthal Germany. Research stays by CES at TU Clausthal were supported by the Alexander von Humboldt Foundation. We appreciate the insightful comments of the two anonymous reviewers that improved the quality of the manuscript and the editorial guidance of the Section Editor Chris Poole.

Author contributions NKF carried out the field studies, sampling and drafted the first version of the manuscript with BRN, AV and ANF who also took part in the petrographic studies and data synthesis. CES and EMS designed the project, coordinated sample analyses and together with EM who did the gold analyses, funded and supervised the development of the manuscript. All authors read and approved the manuscript.

Funding The authors have not disclosed any funding.

Declarations

Conflict of interest The authors have no relevant financial or non-financial interests to disclose.

References

1. Pesquera A, Torres-Ruiz J, Gil-Crespo PP, Jiang S-Y (2005) Petrographic, chemical and B-isotopic insightsinto the origin of tourmaline-rich rocks and boron recycling in the Martinamor antiform (central Iberian zone, Salamanca, Spain). J Petrol 46:1013–1044. https://doi.org/10.1093/petrology/egi009
2. Dutrow BL, Henry DJ (2011) Tourmaline: a geologic DVD. Elements 7:301–306. https://doi.org/10.2138/am.2011.3636
3. Torres-Ruiz J, Pesquera A, Gil-Crespo PP, Velilla N (2003) Origin and petrogenetic implications of tourmaline-rich rocks in the Sierra Nevada (Betic Cordillera, southeastern Spain). Chem Geol 197:55–86. https://doi.org/10.1016/S0009-2541(02)00357-1
4. Marschall HR, Meyer C, Wunder B, Ludwig T, Heinrich W (2009) Experimental boron isotope fractionation between tourmaline and fluid: confirmation from in situ analyses by secondary ion mass spectrometry and from Rayleigh fractionation modelling. Contrib Miner Petrol 158:675–681. https://doi.org/10.1144/0016-76492008-042
5. Marschall HR, Jiang SY (2011) Tourmaline isotopes: no element left behind. Elements 7:313–319. https://doi.org/10.2113/gselements.7.5.313
6. van Hinsberg VJ, Henry DJ, Marschall HR (2011) Tourmaline: an ideal indicator of its host environment. Can Mineral 49:1–16. https://doi.org/10.3749/canmin.49.1.1
7. Slack JF, Trumbull RB (2011) Tourmaline as a recorder of ore-forming processes. Elements 7:321–326. https://doi.org/10.2113/gelements.7.5.321
8. Sciuba M, Beaudoin G, Makvandi S (2020) Chemical composition of tourmaline in orogenic gold deposits. Miner Depos. https://doi.org/10.1007/s00126-020-00981-x
9. Xue Y, Campbell IH, Ireland TR, Holden P, Armstrong R (2013) No mass-independent sulfur isotope fractionation in auriferous fluids supports a magmatic origin for Archean gold deposits. Geology 41:791–879. https://doi.org/10.1130/G34186.1
10. Chapman RJ, Mortensen JK, Crawford EC, Lebarge W (2010) Microchemical studies of placer and lode gold in the Klondike District, Yukon, Canada: 1. evidence for a small, gold-rich, orogenic hydrothermal system in the bonanza and Eldorado CreekArea. Econ Geol 105:1369–1392. https://doi.org/10.2113/econgeo.105.8.1369
11. Trumbull RB, Slack JF, Krienitz M-S, Belkin HE, Wiedenbeck M (2011) Fluid sources and metallogenesis in the Blackbird Co–Cu–Au–Bi–Y–REE district, Idaho, USA: insights from major-element and boron isotopic compositions of tourmaline. Can Min 49:225–244. https://doi.org/10.2113/gsecongeo.104.5.713
12. Molnár F, Mänttäri I, O'Brien H, Lahaye Y, Pakkanen L, Johanson B, Käpyaho A, Sorjonen- Ward P, Whitehouse M, Sakellaris G (2016) Boron, sulphur and copper isotope systematics in the orogenic gold deposits of the Archaean Hattu schist belt, eastern Finland. Ore Geol Rev 77:133–162. https://doi.org/10.1016/j.oregeorev.2016.02.012
13. Gigon J, Skirrow RG, Harlaux M, Richard A, Mercadier J, Annesley IR, Villeneuve J (2019) Insights into B Mg-metasomatism at the ranger U deposit (NT, Australia) and comparison with canadian unconformity-related U deposits. Minerals 2019(9):432. https://doi.org/10.3390/min9070432
14. Sunde O, Friis H, Anderson T, Trumbull R, Wiedenbeck M, Lycberg P, Agostini S, Casey WH, Yu P (2020) Borom isotope composition of coexisting tourmaline and hambergite in alkaline and granitic pegmatites. Lithos 352:105293. https://doi.org/10.1016/j.lithos.2019.105293
15. Gauriau J, Harlaux M, André-Mayer AS, Eglinger A, Richard A, Fontaine A, Lefebvre MG, Béziat D, Villeneuve J, Lemarchand D (2020) Chemical and boron isotope composition of tourmaline from the Kiaka orogenic gold deposit (Burkina Faso, West African Craton) as a proxy for ore-forming processes. Miner Deposita, Spinger, https://doi.org/10.1007/s00126-020-01002-7
16. Philipps GN, Powell R (2010) Formation of gold deposits: a metamorphic devolatilization model. J Metam Geol 28:689–718. https://doi.org/10.1111/j.1525-1314.2010.00887.x
17. Goldfarb RJ, Groves DI (2015) Orogenic gold: common or evolving fluid and metal sources through time. Lithos 233:2–26. https://doi.org/10.1016/j.lithos.2015.07.011
18. Tomkins AG (2013) On the source of orogenic gold. Geology 41:1255–1256. https://doi.org/10.1130/focus122013.1
19. Fontaine A, Eglinger A, Ada K, André-Mayer AS, Reisberg L, Siebenaller L, Le Mignot E, Ganne J, Poujol M (2017) Geology of the world-class Kiaka polyphase gold deposit, West African Craton Burkina Faso. J Afr Earth Sci 126:96–122. https://doi.org/10.1016/j.jafrearsci.2016.11.017
20. Asaah AV, Zoheir B, Lehmann B, Frei D, Burgess R, Suh CE (2014) Geochemistry and geochronology of the ~620 Ma gold-associated Batouri granitoids. Cameroon Int Geol Rev 57(11–12):1485–1509. https://doi.org/10.1080/00206814.2014.951003
21. Omang BO, Suh CE, Lehmann B, Vishiti A, Chombong NN, Fon AN, Egbe JA, Shemang EM (2015) Microchemical signature of alluvial gold from two contrasting terrains in Cameroon. J Afr Earth Sci. https://doi.org/10.4236/ijg.2014.59087
22. Vishiti A, Suh CE, Lehmann B, Egbe JA, Shemang EM (2015) Gold grade variation and particle microchemistry in exploration pits of the Batouri gold district. SE Cameroon J Afr Earth Sci 111:1–13. https://doi.org/10.1016/j.jafrearsci.2015.07.010
23. Ateh KI, Suh CE, Shuster J, Shemang EM, Vishiti A, Reith F, Southam G (2021) Alluvial gold in the Bétaré Oya drainage system, east Cameroon. J Sediment Environ 6:201–212. https://doi.org/10.1007/s43217-021-00051-w
24. Tata E, Suh CE, Vishiti A, Shemang EM, Fon AN, Ateh KI, Chombong NN (2018) Wallrock alteration categories and their geochemical signatures in goldbearing Neoproterozoic granitoids, Batouri gold district, southeastern Cameroon. Geochem Explor Environ Anal. https://doi.org/10.1144/geea2016-017
25. Ngatcha RB, Okunlola OA, Suh CE, Ateh KI, Hofmann A (2019) Petrochemical characterization of Neoproterozoic Colomine granitoids, SE Cameroon: implications for gold mineralization. Lithos 344–345:175–192. https://doi.org/10.1016/j.lithos.2019.06.028
26. Ndonfack KIA, Xie Y, Goldfarb R (2021) Gold occurrences of the Woumbou–Colomine–Kette district, eastern Cameroon: ore-forming constraints from petrography, SEM–CL imagery, fluid inclusions, and C-O–H–S isotopes. Min Depos. https://doi.org/10.1007/s00126-021-01050-7
27. Ateh KI, Suh CE, Shemang EM, Vishiti A, Tata E, Chombong NN (2017) New LA-ICP-MS U-Pb ages, Lu-Hf systematics and REE characterization of zircons from a granitic pluton in the Bétaré Oya gold district, SE Cameroon. J Geosci Geomat 5:267–283. https://doi.org/10.12691/jgg-5-6-2
28. Pirajno F (1992) Hydrothermal mineral deposits – Principles and fundamental concepts for the exploration geologist. Springer, Berlin. https://doi.org/10.1007/978-3-642-75671-9
29. Fuh CG (1990) The geochemical and structural controls on gold mineralization in the Colomines area: Pan-African Belt of Eastern Cameroon. In: University of London, UK. Ph.D. thesis
30. Chapman RJ, Mortensen JK (2016) Characterization of gold mineralization in the northern Cariboo gold district, British

Columbia, Canada, through integration of compositional studies of lode and detrital gold with historical placer production: a template for evaluation of orogenic Gold Districts. Econ Geol 111:1321–1345. https://doi.org/10.2113/econgeo.111.6.1321

31. Masson F-X, Beaudoin G, Laurendeau D (2020) Quantification of the morphology of gold grains in 3D using X-ray microscopy and SEM photogrammetry. J Sediment Res 90:286–296. https://doi.org/10.2110/jsr.2020.16
32. Liu H, Beaudoin G (2021) Geochemical signatures in native gold derived from Au bearing ore deposits. Ore Geol Rev. https://doi.org/10.1016/j.oregeorev.2021.104066
33. Fon AN, Cheo Emmanuel Suh CE, Vishiti A, Ngatcha RB, Ngang TC, Shemang EM, Egbe JE, Lehmann B (2021) Gold dispersion in tropical weathering profiles at the Belikombone gold anomaly (Betare Oya gold district), east Cameroon. Geochemistry. https://doi.org/10.1016/j.chemer.2021.125770
34. Ketchaya YK, Dong G, Santosh M, Lemdjou YB (2022) Microchemical signatures of placer gold grains from the Gamba district, northern Cameroon: implications for possible bedrock sources. Ore Geol Rev 141:104640. https://doi.org/10.1016/j.oregeorev.2021.104640
35. Chapman RJ, Mortensen JK, LeBarge WP (2011) Styles of lode gold mineralization contributing to the placers of the Indian River and Black Hills Creek, Yukon Territory, Canada as deduced from microchemical characterization of placer gold grains. Miner Deposita 46:881–903. https://doi.org/10.1007/s00126-011-0356-5
36. Alam M, Li S-R, Santosh M, Yuan M-W (2019) Morphology and chemistry of placer gold in the Bagrote and Dainter streams, northern Pakistan: implications for provenance and exploration. Geol J 54:1672–1687. https://doi.org/10.1002/gj.3262
37. Nguimatsia Dongmo FW, Chapman RJ, Bolarinwa AT, Yongue RF, Banks DA, Olajide-Kayode JO (2019) Microchemical characterization of placer gold grains from the Meyos-Essabikoula area, Ntem complex, southern Cameroon. J Afr Earth Sci 151:189–201. https://doi.org/10.1016/j.jafrearsci.2018.12.006
38. Fuanya C, Bolarinwa AT, Kankeu B, Yongue RF, Ngatcha RB, Tangko TE (2019) Morphological and chemical assessment of alluvial gold grains from Ako'ozam and Njabilobe, southwestern Cameroon. J Afr Earth Sci 154:111–119. https://doi.org/10.1016/j.jafrearsci.2019.03.012
39. Nono GDK, Bongsiysi EF, Tamfuh PA, Abolo AJ, NKehding BF, Kibong NF, Suh CE (2021) Gold deposit type and implication for exploration in the Abiete- Toko Gold District, South Cameroon: constraint from morphology and microchemistry of alluvial gold grains. Heliyon 7(4):e06758. https://doi.org/10.1016/j.heliyon.2021.e06758
40. Ngatcha RB, Suh CE, Kah FN, Shemang EM, Mpelane S (2021) Base metal-enriched gold-quartz veins in the eastern Cameroon goldfields, West-Central Africa. IUGS. https://doi.org/10.18814/epiiugs/2021/021019
41. Toteu SF, Penaye J, Djomani YP (2004) Geodynamic evolution of the Pan-African belt in central Africa with special reference to Cameroon. Can J Earth Sci 41(73–85):5. https://doi.org/10.1139/e03-079
42. Van Schmus WR, Oliveira EP, Da Silva Filho AF, Toteu SF, Penaye J, Guimaraes IP (2008) The Central African Fold Belt Proterozoic Links between the Borborema Province, NE Brazil, and the Central African Fold Belt. Geological. https://doi.org/10.1144/SP294.5
43. Ngako V, Affaton P, Njonfang E (2008) Pan-African tectonics in northwestern Cameroon: implication for the history of western Gondwana. Gondwana Res 14:509–522. https://doi.org/10.1016/j.gr.2008.02.002
44. Milési JP, Toteu SF, Deschamps Y, Feybesse JL, Lerouge C, Cocherie A, Penaye J, Tchameni R, Moloto-A-Kenguemba G, Kampunzu HAB, Nicol N, Duguey E, Leistel JM, Saint-Martin M, Ralay F, Heinry C, Bouchot V, Doumnang Mbaigane JC, Kanda Kula V, Chene F, Monthel J, Boutin P, Cailteux J (2006) An overview of the geology and major ore deposits of Central Africa: explanatory note for the 1: 4,000,000 maps 'Geology and major ore deposits of Central Africa.' J Afr Earth Sci 44:571–659. https://doi.org/10.1016/j.jafrearsci.2005.10.016
45. Tchameni R, Pouclet A, Penaye J, Ganwa AA, Toteu SF (2006) Petrography and geochemistry of the Ngaoundéré Pan-African granitoids in Central North Cameroon: Implications for their sources and geological setting. J Afr Earth Sci 44:511–529. https://doi.org/10.1016/j.jafrearsci.2005.11.017
46. Ngako V, Affaton P, Nnange JM, Njanko JT (2003) PanAfrican tectonic evolution in central and southern Cameroon: transpression and transtension during sinistral shear movements. J Afr Earth Sci 36:207–214. https://doi.org/10.1016/S0899-5362(03)00023-X
47. Suh CE, Lehmann B, Mafany GT (2006) Geology and geochemical aspects of lode gold mineralization at Dimako-Mboscorro, SE Cameroon. Geochem Explor Environ Anal 6:295–309. https://doi.org/10.1144/1467-7873/06-110
48. Toteu SF, Penaye J, Deloule E, Van Schmus WR, Tchameni R (2006) Diachronous evolution of volcano-sedimentary basins north of the Congo craton: insights from UP-b ion microprobe dating of zircons from the Poli, Lom and Yaounde Groups (Cameroon). J Afr Earth Sci 44:428–442. https://doi.org/10.1016/j.jafrearsci.2005.11.011
49. Kankeu B, Greiling RO, Nzenti JP (2009) Pan-african strike-slip tectonics in eastern cameroon magnetic fabrics (AMS) and structures in the Lom Basin and its gneissic basement. Precambrian Res 174:258–272. https://doi.org/10.1016/S0899-5362(03)00023-X
50. Bouyo Houketchang M, Penaye J, Njel UO, Moussango API, Sep JPN, Nyama BA, Wassouo WJJ, Abate ME, Yaya F, Mahamat A, Hao Ye, Wu F (2016) Geochronological, geochemical and mineralogical constraints of emplacement depth of TTG suite from the Sinassi Batholith in the Central African Fold Belt (CAFB) of northern Cameroon: implications for tectono-magmatic evolution. J Afr Earth Sci 116:9–41. https://doi.org/10.1016/j.jafrearsci.2015.12.005
51. Ganwa AA, Siebel W, Frisch W, Shang Kongnyuy C (2011) Geochemistry of magmatic rocks and time constraints on deformational phases and shear zone slip in the Méiganga area, central Cameroon. Int Geol Rev 3:759–784
52. Vishiti A, Suh CE, Lehmann B, Shemang EM, Ngome NL, Nshanji NJ et al (2017) Mineral chemistry, bulk rock geochemistry, and S-isotope signature of lode-gold mineralization in the Bétaré Oya gold district, south-east Cameroon. Geol J 53:2579–2596. https://doi.org/10.1002/gj.3093
53. Takodjou Wambo JD, Beiranvand AP, Ganno S, Asimow DP, Zoheir B, Salles R et al (2020) Identifying high potential zones of gold mineralization in a sub-tropical region using Landsat-8 and ASTER remote sensing data: a case study of the Ngoura-Colomines goldfield, Eastern Cameroon. Ore Geol Rev 122:103530. https://doi.org/10.1016/j.oregeorev.2020.103530
54. Goldfarb RJ, Groves DI, Gardoll S (2001) Orogenic gold and geologic time: a global synthesis. Ore Geol Rev 18:1–75. https://doi.org/10.1016/S0169-1368(01)00016-6
55. Soba D, Michard A, Toteu SF, Norman DI, Penaye J, Ngako V, Nzenti JP, Dautel D (1991) U-Pb, Sm–Nd and Rb–Sr dating in the Pan African mobile belt of Eastern Cameroon: upper Proterozoic age of the Lom series. C R Acad Sci 312:1453–1458
56. Ndonfack KIA, Xie Y, Zhong R, Yomeun BS, Cui K, Shan X (2021) Tectonic evolution of neoproterozoic rocks, eastern cameroon: implication for gold mineralization in the Betare Oya and

Woumbou-Colomine-Kette district. Precambrian Res. https://doi.org/10.1016/j.precamres.2021.106475
57. Tata E, Suh CE, Vishiti A, Shemang EM, Ateh KI (2021) Emplacement timing, temperature, and redox conditions of the Kambélé auriferous pluton, Batouri gold District, SE Cameroon. IUGS. https://doi.org/10.18814/epiiugs/2021/021013
58. Ngatcha RB, Suh CE, Okunlola OA, Nunoo S, Ateh KI, Elburg M, Hofmann A (2022) Crustal modelling from Pan-African granites of the Colomine Gold District, SE Cameroon: insights from zircon U-Pb dating and Lu-Hf isotope systematics. J Afr Earth Sci. https://doi.org/10.1016/j.jafrearsci.2021.104441
59. Soba D (1989) La série du Lom: étude géologique et géochronologique d'un bassin volcano-sédimentaire de la chaine panafricaine à l'Est du Cameroun. In: Thèse de doctorat d'Etat. 6. Université Pierre et Marie Curie, Paris, p 198
60. Nkoumbou C, Yonta Ngouné C, Villiéras F, Njopwouo D, Yvon J, Ekodeck GE, Tchoua FM (2006) Découverte de roches à affinite ophiolitiques dans la chaîne panafricaine au Cameroun: les talcschistes de Ngoung, Lamal Pougué et Bibodi Lamal. C R Géosci 338:1167–2117
61. Henry DJ, Novak M, Hawthorne FC, Ertl A, Dutrow BL, Uher P, Pezzotta F (2011) Nomenclature of the tourmaline-super group minerals. Am Min 96:895–913. https://doi.org/10.2138/am.2011.3636
62. Melchiorre EB, Henderson J (2019) Topographic gradients and lode gold sourcing recorded by placer gold morphology, geochemistry, and mineral inclusions in the east fork San Gabriel River, California, U.S.A. Ore Geol Rev 109:348–357. https://doi.org/10.1016/j.oregeorev.2019.04.022
63. Hallbauer DK, Utter T (1977) Geochemical and morphological characteristics of gold particles from recent river deposits and the fossil placer of the Witwatersrand. Miner Depos 12:293–306. https://doi.org/10.1007/BF00206168
64. Henry DJ, Guidotti CV (1985) Tourmaline as a petrogenetic indicator mineral: an example from the staurolite-grade metapelites of NW Maine. Am Min 70:1–15
65. Yardley BWD, Rochelle CA, Barnicoat AC, Lloyd GE (1991) Oscillatory zoning in metamorphic minerals: an indicator of infiltration metasomatism. Mineral Mag 55:357–365. https://doi.org/10.1144/0016-76492008-101
66. Taylor BE, Slack JF (1984) Tourmalines from Appalachian-Caledonian massive sulfide deposits: textural, chemical, and isotopic relationships. Econ Geol 79:1703–1726. https://doi.org/10.2113/gsecongeo.79.7.1703
67. Qiu KF, Yu HC, Hetherington C, Huang YQ, Yang T, Deng D, J., (2021) Tourmaline composition and boron isotope signature as a tracer of magmatic-hydrothermal processes. Am Mineral. https://doi.org/10.2138/am-2021-7495
68. Bozkaya Ö, Baksheev IA, Hanilçi N, Bozkaya G, Prokofiev VY, Özta Y, Banks DA (2020) Tourmaline composition of the kisladag porphyry au deposit, western Turkey: implication of epithermal overprint. Minerals 10:789. https://doi.org/10.3390/min10090789
69. Cheng L, Zhang C, Yang X (2020) Petrogenesis of deformed tourmaline leucogranite in the Gurla Mandhata metamorphic core complex, Southwestern Tibet. Lithos. https://doi.org/10.1016/j.lithos.2020.105533
70. Montenegro T, Wul J (2021) Chemical and boron isotope composition of tourmaline from pegmatites and their host rocks, Sierra de san Luis, Argentina. Can Mineral 59:467–494. https://doi.org/10.3749/canmin.2000072
71. Lambert-Smith JS, Rocholl A, Treloar PJ, Lawrence DM (2016) Discriminating fluid source regions in orogenic gold deposits using B-isotopes. Geochim Cosmochim Acta 194:57–76. https://doi.org/10.1016/j.gca.2016.08.02510.1016/j.gca.2016.08.025
72. Suh CE (2008) Sulphide microchemistry and hydrothermal fluid evolution in quartz veins, Batouri gold district (southeast Cameroon). J Camer Acad Sci 8:19–30. https://doi.org/10.2113/gsemg.17.3-4.197
73. Chapman R, Mileham T, Allan M, Mortensen J (2017) A distinctive Pd-Hg signature in detrital gold derived from alkalic Cu-Au porphyry systems. Ore Geol Rev 83:84–102. https://doi.org/10.1016/j.oregeorev.2016.12.01
74. Trumbull RB, Slack JF (2018) Boron isotopes in the continental crust: granites, pegmatites, felsic volcanic rocks, and related ore deposits. In: Marschall H, Foster G (Eds) Boron isotopes, advances in isotope geochemistry. Springer International Publishing AG 2018, pp 249–272. https://doi.org/10.1007/978-3-319-64666-4_10.
75. Li YC, Chen HW, Wei HZ, Jiang SY, Palmer MR, van de Ven TGM, Hohl S, Lu JJ, Ma J (2020) Exploration of driving mechanisms of equilibrium boron isotope fractionation in tourmaline group minerals and fluid: a density functional theory study. Chem Geol 536:119466. https://doi.org/10.1016/j.chemgeo.2020.119466
76. Hazarika P, Upadhyay D, Mishra B, Borah P, Abhinay K (2021) Modelling B-release and isotopic fractionation during metamorphic dehydration of basalt and pelite: implications for the source of mineralizing fluid in greenstone-hosted orogenic gold deposits. Geochim Cosmochim Acta 304(2021):83–100. https://doi.org/10.1016/j.gca.2021.04.019